

Effective electrodiffusion equation for non-uniform nanochannels

Umberto Marini Bettolo Marconi, Simone Melchionna, and Ignacio Pagonabarraga

Citation: *J. Chem. Phys.* **138**, 244107 (2013); doi: 10.1063/1.4811516

View online: <http://dx.doi.org/10.1063/1.4811516>

View Table of Contents: <http://jcp.aip.org/resource/1/JCPSA6/v138/i24>

Published by the AIP Publishing LLC.

Additional information on J. Chem. Phys.

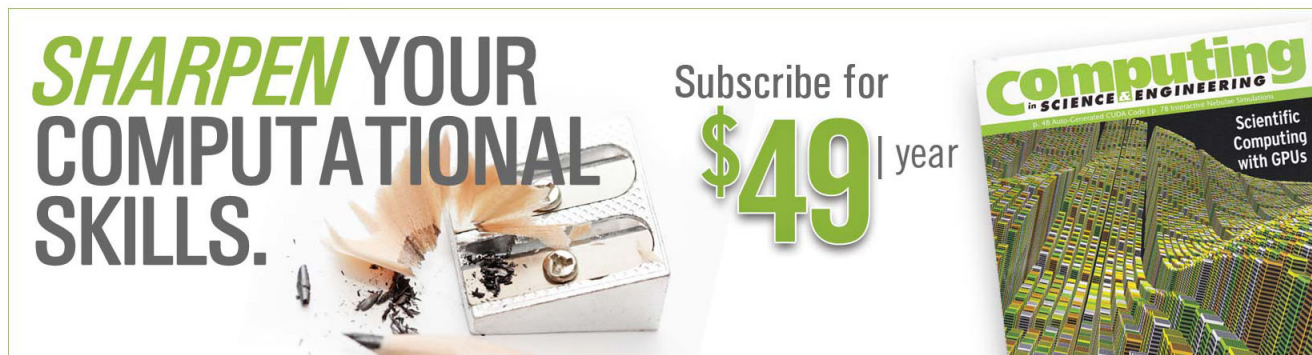
Journal Homepage: <http://jcp.aip.org/>

Journal Information: http://jcp.aip.org/about/about_the_journal

Top downloads: http://jcp.aip.org/features/most_downloaded

Information for Authors: <http://jcp.aip.org/authors>

ADVERTISEMENT



**SHARPEN YOUR
COMPUTATIONAL
SKILLS.**

Subscribe for
\$49 | year

Computing
in **SCIENCE & ENGINEERING**
Scientific
Computing
with GPUs

Effective electrodiffusion equation for non-uniform nanochannels

Umberto Marini Bettolo Marconi,¹ Simone Melchionna,² and Ignacio Pagonabarraga³

¹*Scuola di Scienze e Tecnologie, Università di Camerino, Via Madonna delle Carceri, 62032 Camerino, Italy*

²*CNR-IPCF, Consiglio Nazionale delle Ricerche, Dipartimento di Fisica, Università La Sapienza, 00185 Rome, Italy*

³*Departament de Física Fonamental, Universitat de Barcelona, C. Martí i Franques, 1 08028-Barcelona, Spain*

(Received 19 April 2013; accepted 5 June 2013; published online 27 June 2013)

We derive a one-dimensional formulation of the Planck-Nernst-Poisson equation to describe the dynamics of a symmetric binary electrolyte in channels whose section is nanometric and varies along the axial direction. The approach is in the spirit of the Fick-Jacobs diffusion equation and leads to a system of coupled equations for the partial densities which depends on the charge sitting at the walls in a non-trivial fashion. We consider two kinds of non-uniformities, those due to the spatial variation of charge distribution and those due to the shape variation of the pore and report one- and three-dimensional solutions of the electrokinetic equations. © 2013 AIP Publishing LLC. [<http://dx.doi.org/10.1063/1.4811516>]

I. INTRODUCTION

The study of electric transport properties of ions in pores of nanometric transverse section is a problem of capital importance in many different areas of Biology, Chemistry, Engineering, Physics, and has important technological applications. At the nanoscale, the Debye screening length becomes in the case of dilute electrolytic solutions larger than the typical channel width so that any clear distinction between surface-like and bulk-like region disappears and the properties of the channel are mainly controlled by the surface charge.¹ The theoretical study of electrokinetic phenomena at these scales and in heterogeneous media poses a number of theoretical and computational challenges.² If the channel width is of the order of magnitude of the Debye length, the double layers generated by the presence of surface charge at the walls overlap and the solution inside is prevalently formed by counter-ions. Thus, it is possible to use the surface charge, or the channel geometry,³ to control the concentration of ions inside the channel⁴⁻⁶ with applications to devices.

The time evolution of the concentrations and electric field are reasonably well described by the Planck-Nernst-Poisson (PNP) model, which represents the workhorse of studies in this important field. It combines the Fick diffusion law with the migration effect induced by the electric field produced by the charges either fixed at the boundaries of the system or moving through the solvent. One also assumes that the electric field corresponds to the one produced by a continuous charge distribution obtained by thermally averaging over the instantaneous charge configurations. Numerical solutions of the stationary three-dimensional (3D) PNP problem are discussed in the vast literature on the subject, but it is often desirable to have an even simpler description in terms of a reduced number of coordinates. There have already been a number of previous studies investigating how to treat the dynamics of electrolyte solutions in heterogeneous media.^{7,8} However, in these cases the homogenization procedure considered scales larger than the single pore and the resulting theory was then an ef-

fective medium approximation to describe electrodiffusion at larger scales, in, e.g., porous tissues, membranes, and porous rocks. Other authors, instead, have considered very specific geometries⁹⁻¹¹ to study the rectification of the ionic currents restricted to conical pores by means of a one-dimensional reduction.

In some cases, using the symmetry of the problem and the fact that gradients are negligible in some specific directions it is possible to obtain a one-dimensional effective representation thus reducing the computational effort. In fact, in many systems of interest, such as long tiny channels, the motion basically occurs in a single direction and one may seek a method to reduce the three-dimensional PNP equations to a one-dimensional effective description.^{12,13} In the case of a channel of uniform section such a reduction is simpler than in the case of channels of varying section, whereby the procedure requires a series of additional approximations. Such a program was originally carried out by Jacobs¹⁴ and continued by several authors¹⁵⁻¹⁸ in the case of standard diffusion problems. The methods used by these authors are basically homogenization techniques, by which one eliminates the dependence of some observables on some coordinates, using their slow variation in space. However, the purpose of the present paper is somehow different from the one which motivated the previous authors who were interested in investigating the transient diffusion process in non-uniform channels. Our scope is to analyze how the steady state properties are influenced by the geometry. A second important difference consists in the fact that we apply the homogenization technique to the PNP electrokinetic equations describing the flow of electrolyte solutions in narrow channels of variable width. The derivation of an effective, simplified, equation for the dynamics of charged species along a channel with general geometry will provide physical insight in electrodiffusion in complex geometries.

The present paper is organized as follows: in Sec. II we derive the PNP equations from a free energy approach,

and perform the reduction of the equations from three-dimensional space to one-dimensional space for a axisymmetric system. In Sec. III we solve the full set of one-dimensional equations by numerical methods and compare these results with those obtained by solving the three-dimensional Lattice Boltzmann (LB) equation for a ternary charged mixture composed of two ionic species and a solvent species. Finally, in Sec. IV we discuss the results and present some conclusions.

II. A SIMPLE DERIVATION OF THE PNP SYSTEM AND ONE-DIMENSIONAL REDUCTION

We first derive the PNP equations in the framework of Dynamic Density Functional Theory (DDFT).¹⁹ We assume the following free energy functional describing two oppositely charged species of charges $\pm ze$ in the presence of a quiescent, structureless solvent of dielectric constant ϵ , and of a fixed charge distribution $q_e(\mathbf{r})$:

$$\mathcal{F}[n^+, n^-, \phi] = \int d\mathbf{r} \left[(k_B T \sum_{\alpha=\pm} n^\alpha(\mathbf{r}) [\ln(n^\alpha(\mathbf{r}) \Lambda_\pm^3) - 1] + e[z(n^+(\mathbf{r}) - n^-(\mathbf{r})) + q_e(\mathbf{r})]\phi(\mathbf{r}) - \frac{\epsilon}{2}(\nabla\phi(\mathbf{r}))^2 \right], \quad (1)$$

where we have introduced the electric potential ϕ in order to have a local formulation of the theory²⁰ and Λ_\pm represents the thermal de Broglie wavelength of the two ionic species. The free energy, \mathcal{F} , contains only ideal gas entropic contributions and the Coulomb interaction term. Within the DDFT one describes the relaxation of the ionic densities and the electric potential by the following set of governing equations:

$$\frac{\partial n^\pm(\mathbf{r}, t)}{\partial t} = \frac{1}{\gamma^\pm} \nabla \cdot \left(n^\pm(\mathbf{r}, t) \nabla \frac{\delta \mathcal{F}[n^+, n^-]}{\delta n^\pm(\mathbf{r}, t)} \right), \quad (2)$$

which can be regarded as a continuity equation for the individual species, with partial currents given by

$$\mathbf{J}^\pm(\mathbf{r}, t) = -\frac{1}{\gamma^\pm} \left(n^\pm(\mathbf{r}, t) \nabla \frac{\delta \mathcal{F}[n^+, n^-]}{\delta n^\pm(\mathbf{r}, t)} \right). \quad (3)$$

Here γ^\pm are coefficients characterizing the friction of the ions with the solvent, so that the diffusion coefficients D^\pm follow from the Einstein relation $D^\pm = \frac{k_B T}{\gamma^\pm}$. Upon differentiating the free energy (1) at fixed electric potential we obtain the explicit expression

$$\frac{\delta \mathcal{F}[n^+, n^-]}{\delta n^\pm(\mathbf{r}, t)} = k_B T \ln n^\pm(\mathbf{r}, t) \pm ze\phi(\mathbf{r}, t) \quad (4)$$

and after substituting in Eq. (2) we arrive at the following driven diffusion equation:

$$\frac{\partial n^\pm(\mathbf{r}, t)}{\partial t} = D^\pm \nabla \cdot \left(\nabla n^\pm(\mathbf{r}, t) \mp \frac{ze n^\pm(\mathbf{r}, t)}{k_B T} \mathbf{E}(\mathbf{r}, t) \right). \quad (5)$$

For later reference we shall specify the Debye length

$$\lambda_D = \sqrt{\frac{\epsilon k_B T}{2z^2 e^2 n_b}},$$

where n_b is the bulk value of the densities of the two ionic species. The governing equation for the electric field $\mathbf{E} = -\nabla\phi$ is obtained by functionally differentiating (1) with respect to ϕ at constant densities

$$\nabla \cdot \mathbf{E}(\mathbf{r}, t) = \frac{ze}{\epsilon} (n^+(\mathbf{r}, t) - n^-(\mathbf{r}, t)). \quad (6)$$

The Poisson equation (6) must be supplemented by the boundary condition $\mathbf{E} \cdot \mathbf{n}(x) = \frac{\Sigma(x)}{\epsilon}$.

Equations (5) and (6) constitute the Poisson-Nernst-Planck model. Here we are interested in those cases where the dynamics occurs mainly along a single direction, say the x -direction. Convenient observables depending only on x are the sectionally averaged densities, for which one can derive simple evolution equations. The reduction in dimensionality from 3D to 1D is based on the assumption, reasonable for narrow channels, that all motions perpendicular to the axis reach equilibrium more rapidly than those along it. The method can be generalized to the case of non-uniform confining geometries where the resulting evolution equations contain extra terms, interpreted as entropic forces,¹⁵ due to tendency of the particles to fill uniformly the space. In fact, narrower sections contain a number of particles per unit length smaller than wider ones.

Let us consider a 3D system with axial symmetry along the x direction bounded by a surface described by the shape function $R = R(x)$ and assume that the particles can move only in the inner space, so that $n(x, r) = 0$, if $r > R(x)$. We define the sectional average of a generic field $a(x, r)$ as

$$\langle a(x) \rangle = \frac{2}{R^2(x)} \int_0^{R(x)} dr r a(x, r), \quad (7)$$

where r is the distance from the x axis. By applying the averaging operator $\langle \cdot \rangle$, to the equation for the current $\mathbf{J}^\pm(x)$, one obtains the following expression for its x -component:

$$\langle J_x^\pm(x) \rangle = -D^\pm \left(\frac{d}{dx} \langle n^\pm(x) \rangle + \frac{2R'(x)}{R(x)} (\langle n^\pm(x) \rangle - n^\pm(x, R)) \right) \pm \mu^\pm \langle E_x(x) \rangle \langle n^\pm(x) \rangle, \quad (8)$$

where in the last term we have approximated the average of the forcing term in Eq. (5) by the product of averages. If we further assume that the density profile in the transverse direction varies slowly, so that its local value at the wall, $r = R$, can be approximated by its sectional average, the coefficient of the derivative of $R(x)$ vanishes. Assuming the confining walls to be impenetrable, the component of the current parallel to the normal \mathbf{n} , must vanish at the lateral boundaries $\mathbf{J}^\pm(x, R) \cdot \mathbf{n} = 0$. Under stationary conditions the currents are subject to the zero divergence conditions $\nabla \cdot \mathbf{J}^\pm(\mathbf{r}) = 0$, so that for a channel of variable section the quantity $I^\pm = \frac{\langle J_x^\pm(x) \rangle}{D^\pm} \pi R^2(x)$ must be constant. In order to integrate Eq. (8) we define a new concentration variable

$$c^\pm(x) \equiv \pi R^2(x) \langle n^\pm(x) \rangle \quad (9)$$

and write the 1D-PNP equation as

$$\frac{dc^\pm(x)}{dx} - 2 \frac{R'(x)}{R(x)} c^\pm(x) \mp \frac{ze \langle E_x(x) \rangle}{k_B T} c^\pm(x) = -I^\pm. \quad (10)$$

The r.h.s. of Eq. (10) has the simple interpretation of (minus) the current generated by a gradient of concentration $c(x)$, by the entropic force associated with the area variation of each section plus a force due to the electric field. If $\langle E_x \rangle = 0$, the current, I^\pm , vanishes when $c^\pm(x)/\pi R^2(x) = \langle n^\pm(x) \rangle = \text{const}$.

By applying the averaging operation to the Poisson equation we obtain

$$\frac{2}{R^2(x)} \int_0^{R(x)} dr r \frac{\partial E_x}{\partial x} = \frac{ze}{\epsilon} \langle (n^+ - n^-) \rangle - \frac{2}{R(x)} E_r(x, R) \quad (11)$$

and using the identity

$$\frac{2}{R^2(x)} \int_0^{R(x)} dr r \frac{\partial E_x}{\partial x} = \frac{d\langle E_x(x) \rangle}{dx} + \frac{2R'(x)}{R(x)} (\langle E_x \rangle - E_x(x, R)), \quad (12)$$

we can write

$$\begin{aligned} & \frac{d\langle E_x(x) \rangle}{dx} + \frac{2R'(x)}{R(x)} \langle E_x \rangle \\ &= \frac{ze}{\epsilon} \langle (n^+ - n^-) \rangle - \frac{2}{R(x)} (E_r(x, R) \\ & \quad - R'(x) E_x(x, R)). \end{aligned} \quad (13)$$

Finally, we consider the relation between the radial, E_r , and the longitudinal components E_x , of the electric field at the boundary and the surface charge:

$$\begin{aligned} \mathbf{E} \cdot \mathbf{n}(x) &= -[E_r(x, R) - E_x(x, R)R'(x)] \frac{1}{\sqrt{1 + (R'(x))^2}} \\ &= \frac{\Sigma(x)}{\epsilon}. \end{aligned} \quad (14)$$

To conclude the sectional averaging of the Poisson equation (6) yields the following result:

$$\begin{aligned} & \frac{d\langle E_x(x) \rangle}{dx} + 2 \frac{R'(x)}{R(x)} \langle E_x(x) \rangle \\ &= \frac{1}{\epsilon \pi R^2(x)} (ze(c^+(x) - c^-(x)) \\ & \quad + 2\pi R(x) \Sigma(x) \sqrt{1 + (R'(x))^2}), \end{aligned} \quad (15)$$

where the term $\Sigma(x) \sqrt{1 + (R'(x))^2}$ represents the product of the surface area charge density with the line length of the boundary. Such a correction due to the line length has usually been neglected on account of the small effect in the case of nearly flat interfaces. The presence of the second term on the left hand side of Eq. (15) is due to the sectional averaging and has the form predicted by Eisenberg and co-workers.^{21,22} Formula (15) reflects the fact that in the absence of free charges the quantity $\langle E_x(x) \rangle \pi R^2(x)$ is constant throughout the system. Let us remark that the equation for the electric field is one-dimensional and the surface charge appears now directly in the 1D Poisson equation as a source term as a result of the homogenization procedure.

Notice that we can also define a one-dimensional electric potential $\bar{\psi}(x)$ such that $\langle E_x(x) \rangle = -\frac{d\bar{\psi}(x)}{dx}$ which, however, is not the sectional average $\langle \phi \rangle$ of the true potential $\phi(x, r)$.

III. PERFORMANCE OF THE ONE-DIMENSIONAL PNP REDUCED MODEL

The purpose of the present section is to assess the validity of the 1D-PNP equations (10) and (15) by comparing the numerical solutions with those obtained by solving the full three-dimensional problem. For the latter, the electrokinetic equations will be solved numerically in the framework of the LB method. The 3D system used in the LB comparison is composed by a ternary mixture of positively and negatively charged point particles immersed in a solvent of neutral particles. The three types of particles move in a continuum dielectric medium of uniform permeability ϵ .

The system evolves according to the following kinetic equations for the one-particle phase space distributions $f^\alpha(\mathbf{r}, \mathbf{v}, t)$ of each species α :

$$\begin{aligned} & \frac{\partial}{\partial t} f^\alpha(\mathbf{r}, \mathbf{v}, t) + \mathbf{v} \cdot \nabla_r f^\alpha(\mathbf{r}, \mathbf{v}, t) - \frac{ez^\alpha \nabla_r \psi(\mathbf{r}, t)}{m^\alpha} \\ & \cdot \frac{\partial}{\partial \mathbf{v}} f^\alpha(\mathbf{r}, \mathbf{v}, t) = -\omega [f^\alpha(\mathbf{r}, \mathbf{v}, t) - n^\alpha(\mathbf{r}, \mathbf{v}, t) \phi_M(\mathbf{r}, \mathbf{v}, t)], \end{aligned} \quad (16)$$

where

$$\phi_M(\mathbf{r}, \mathbf{v}, t) = \left[\frac{m}{2\pi k_B T} \right]^{3/2} \exp \left[-\frac{m(\mathbf{v} - \mathbf{u}(\mathbf{r}, t))^2}{2k_B T} \right] \quad (17)$$

is the Maxwell-Boltzmann distribution peaked around the common fluid velocity, \mathbf{u} (see Ref. 23).

From the distribution functions f^α , also called populations, we extract the local densities $n^\alpha(\mathbf{r}, t) = \int d\mathbf{v} f^\alpha(\mathbf{r}, \mathbf{v}, t)$ and the currents are obtained as $J^\alpha(\mathbf{r}, t) = \int d\mathbf{v} \mathbf{v} f^\alpha(\mathbf{r}, \mathbf{v}, t)$, and thus the common velocity is given by $\mathbf{u} = \sum_\alpha J^\alpha(\mathbf{r}, t) / \sum_\alpha n^\alpha$. We determine the electric field \mathbf{E} by solving numerically the 3D Poisson equation (6) by means of a SOR (Successive over-relaxation) algorithm.²⁴ In addition, we fix the diffusion coefficients to be the same for each species and equal to $D^\alpha = k_B T / \omega m^\alpha = 1$, where ω is the relaxation frequency featuring in Eq. (17). The discretized version of Eq. (16), which

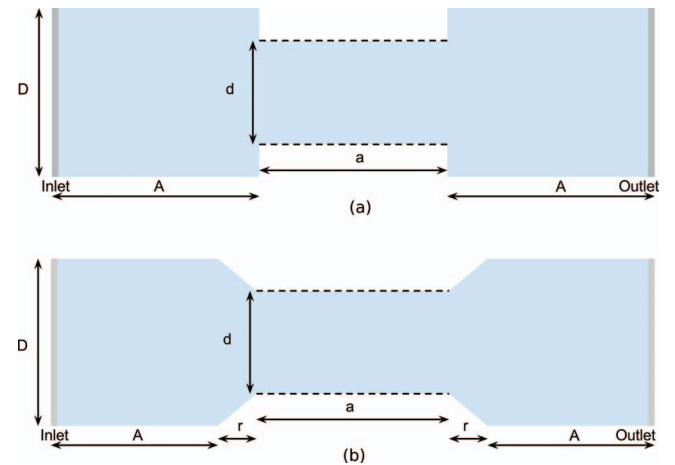


FIG. 1. Geometries used in the numerical tests, with the set-ups denoted as A (upper) and B (lower). The dashed lines indicate the location of the surface charge. The potential tension is applied between the inlet and outlet regions. Throughout the text, the labels D , d , A , a , and r are expressed in lattice units.

is the essence of the LB method, is not reported here. The interested reader can find the details of the complete numerical scheme in Refs. 25–28, where the more general situation when the finite size of the ions is relevant is also discussed. The model we will use is analogous to other LB approaches to model electrokinetics.^{29,30} In the following we use lattice units to express the density and the electric potential. Given the lattice spacing Δx , the dimensionless Debye length and number density are defined $\lambda_D = \tilde{\lambda}_D \Delta x$ and $n = \tilde{n} \Delta x^3$, where $\tilde{\lambda}_D$ and \tilde{n} are the dimensional counterparts. Similarly, $\Sigma = \tilde{\Sigma} \Delta x^2 / e$, $\phi = e\tilde{\phi} / k_B T$, and $\Delta V = e\tilde{\Delta V} / k_B T$ are the dimensionless surface charge, electric potential, and applied tension, respectively.

The studied systems are depicted in Fig. 1 and consist of two reservoirs connected by a straight channel with the three compartments having cylindrical symmetry with radius $R(x)$. System A contains a straight cylindrical channel with a sharp discontinuity in the radius profile $R(x)$ at the channel openings, it is therefore quite challenging to reproduce the 3D charge distribution and currents within the 1D-PNP

framework. System B, instead, contains two ramps at the channel openings that could ameliorate in principle the quality of the 1D-PNP solution, by reducing the discontinuities in $R(x)$. The inner surface of the channels has a surface charge density $\Sigma(x)$ that is uniform for both systems inside the channel for both systems and equal to -2×10^{-4} . For a lattice spacing $\Delta x = 0.1$ nm, this surface charge density is about one order of magnitude smaller than the value typical of a SiN channel.³¹

In the simulations, a potential difference is applied across the system at the left and right extremes of the system, hereafter named inlet and outlet, respectively. At these extremes, x_I and x_O , we fix the electrostatic potential, ϕ_I and ϕ_O , as

$$\phi(x_I, y, z) = \phi_I \quad \phi(x_O, y, z) = \phi_O \quad (18)$$

and we assume all species to have the density fixed by their bulk values at the electrodes

$$n^\pm(x_I, y, z) = n^\pm(x_O, y, z) = n_b^\pm. \quad (19)$$

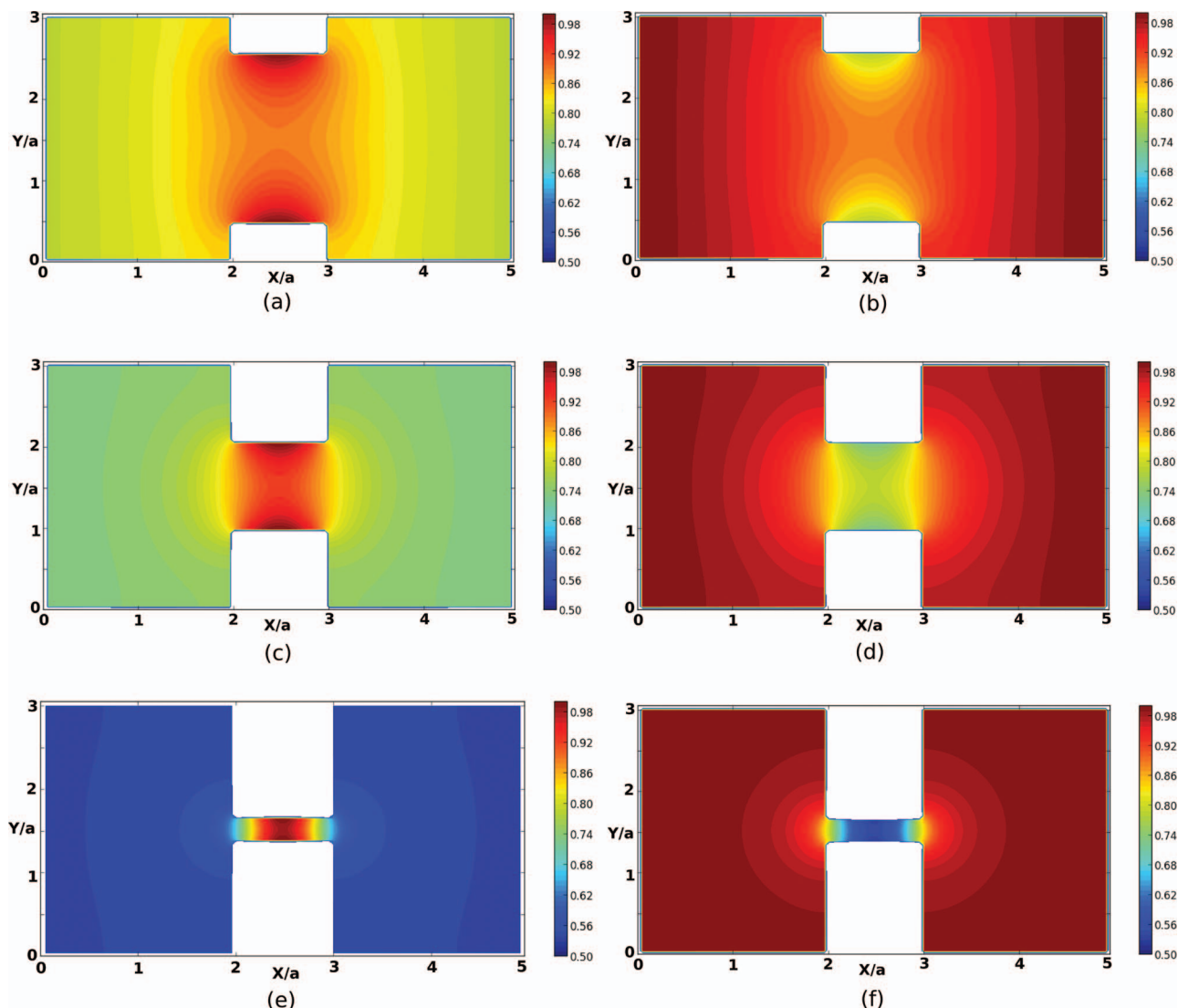


FIG. 2. Normalized density of counter-ions (left) and co-ions (right plot) for system A for wide (plots (a) and (b) with $d = 40$, $D = 60$, $a = 20$, and $A = 40$), medium (plots (c) and (d) with $d = 20$, $D = 60$, $a = 20$, and $A = 40$), and small (plots (e) and (f) with $d = 10$, $D = 60$, $a = 20$, and $A = 40$) channels, with $\Delta V = 10^{-2}$.

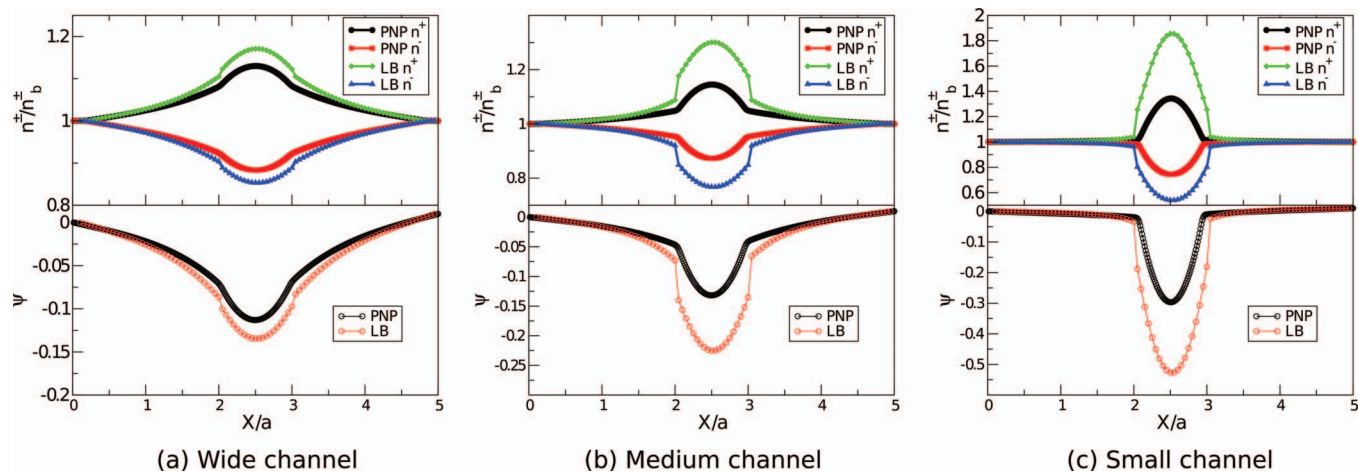


FIG. 3. Comparison of 1D-PNP and 3D-LB longitudinal profiles of the density (upper panels) and the potential (lower panels). The geometries and parameters are as in Fig. 2.

The 1D-PNP equations (10) and (15) are handled numerically by using conventional methods, where Eqs. (10) and (15) are solved by a SOR relaxation methods on a one-dimensional mesh, with a resolution of 100 mesh points per Debye length. In particular, Eq. (10) is considered by taking one more spatial derivative so to avoid a shooting method for the currents I^{\pm} . In order to improve the accuracy of the solution, the equations are rewritten via an exponential transform, so to alleviate any rapidly varying function.

In terms of the 3D-LB numerical scheme, in order to impose the densities at the electrodes, we choose appropriately the populations such as to recover the corresponding zeroth moments. At the same time, the first moments (the currents) should be left untouched by the boundary method. At the extremal regions, this problem consists of completing the pop-

ulations with contributions stemming from the incoming (at the inlet) and outgoing (at the outlet) missing information. To this end, we apply the completion scheme of Ref. 32, which imposes the non-equilibrium part of the populations for the contributions directed along $+x$ and $-x$ to be equal.

The contour plots of the 3D-LB densities are reported in Fig. 2 for pores of different diameters and undergoing the action of an external tension. For the same systems, in Fig. 3 we compare the sectionally averaged, longitudinal profiles of the densities and the electrostatic potential. From the data, 3D-LB and 1D-PNP obey similar general trends, with a build-up of counter-ions with a characteristic bell-shape inside the channel, whereas concentration polarization develops in the reservoir regions. The latter is a manifestation of the electrostatic attraction of counter-ions towards the charged

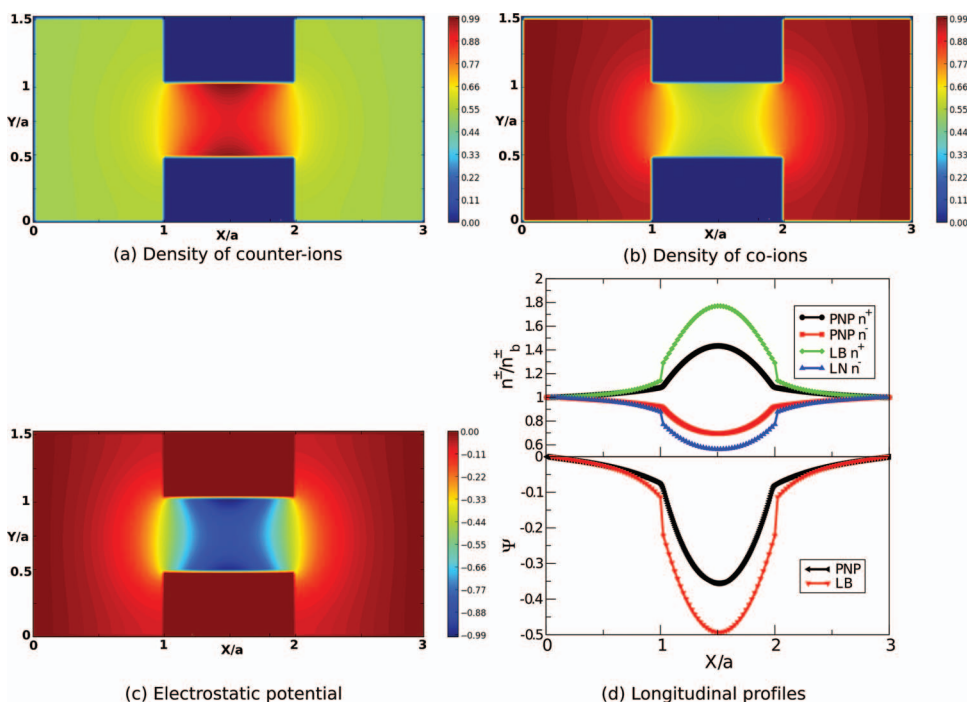


FIG. 4. Normalized density of electrolytes, electrostatic potential, and longitudinal profiles for system A ($d = 20$, $D = 60$, $a = 40$, and $A = 40$), with $\Delta V = 0$.

channel, contrasted by the external walls of the reservoir. The most relevant difference between 3D-LB and 1D-PNP is the amount of counter-ion build-up and co-ion depletion in the channel region. In particular, the 3D-LB data show a discontinuity of the charge profiles at the channel openings, apparently due to the strong confining forces acting on the electrolytes.

From Figs. 2 and 3 it is worth noting the increase of counter-ion build-up and co-ion depletion as the channel diameter is reduced. The narrower is the channel, the larger is the difference in profiles between the PNP and LB solutions. At the same time, the charge distribution in the reservoirs is long ranged and has hemispherical shape. Such long-range modulation is the effect of the strong confinement of the electric field lines as they squeeze in the channel region, usually referred to as entrance/exit effects since any particle ap-

proaching/exiting the channel will feel a substantial modulation in the potential already at long distance from the channel opening. The same type of distribution is observed in Fig. 4 where the channel is taken to be longer than the Debye length ($a = 40$, $\lambda_D = 20$).

Due to the long-ranged effect of concentration polarization, we considered a system with more extended reservoirs to avoid spurious finite size effects. The contour plots of the 3D LB densities and the comparison of the longitudinal profiles are reported in Fig. 5. Once more, 3D-LB and 1D-PNP obey similar general trends, with a bell-shaped build-up of counter-ion in the pore region. Now, concentration polarization has a minor effect nonetheless, the same type of charge discontinuity is observed in the 3D simulation, ruling out the possibility that the gap between 3D-LB and 1D-PNP is induced by the reservoir regions. Accordingly, we keep

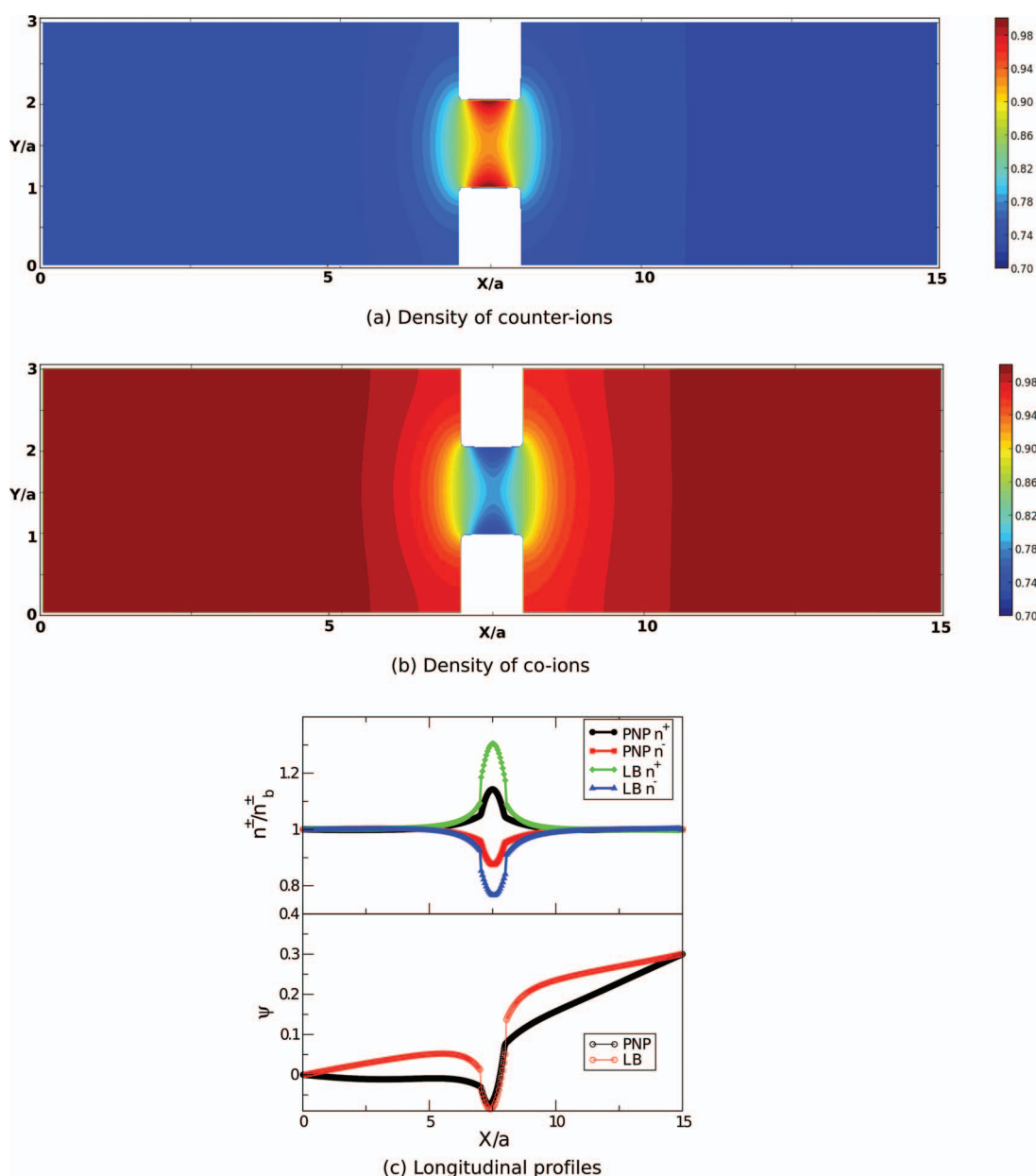


FIG. 5. Density of electrolytes normalized by the maximum value ((a) and (b)). (c) compares the 1D-PNP and 3D-LB longitudinal profiles of the density (plot (c), upper) and the potential (plot (c), lower) for system A ($d = 20$, $D = 60$, $a = 20$, and $A = 140$), with $\Delta V = 10^{-1}$.

the original reservoir size in the rest of the computational studies.

The differences in the solution obtained with 1D-PNP and 3D-LB at the pore mouths can have different causes and further inspection is required. The neglect of charge polarization in the transverse direction at PNP level can be at the origin of such differences. However, another cause of the differences can be the sharp discontinuities in the entropic forces, via the profile $R(x)$, at the channel openings. It is possible that the homogenized solution fails in capturing such strong axial modulation. To explore this possibility, in Fig. 6 we report the profiles of the counter-ions density and electrostatic potential obtained with system A and system B. The two geometries have the same extension of the reservoirs and pore geometry, and the same surface charge. From the plot, it is apparent that the differences between 1D-PNP and 3D-LB in the electrostatic potential are still marked, however, the 1D-PNP solution for system B shows a clear trend to increase the charge build-up in the channel region. Therefore, the 1D-PNP

and 3D-LB solutions are more similar for system B than for system A.

Quantitative predictions of the potential and density profiles induced by sharp changes of the wall profile $R(x)$ is a delicate matter since, as reported by different authors, homogenization procedures work well only for smooth variations of the wall profiles.^{16,17} The one-dimensional PNP predictions against exact three-dimensional LB solutions in the case of free diffusion in channels of variable section were found to work well for slow variations of the channel profile.

Finally, the validation of the 1D-PNP effective equations requires studying the attitude to ionic transport as compared to the 3D-LB solution. A simplified theory that can quantitatively predict ionic conductance, $G = I/\Delta V$, where I is the electric current and ΔV is the potential difference between the two extremes, is highly desirable. For this reason we have computed both the charge distribution of electrolytes and the ionic conductance at different values of the Debye length.

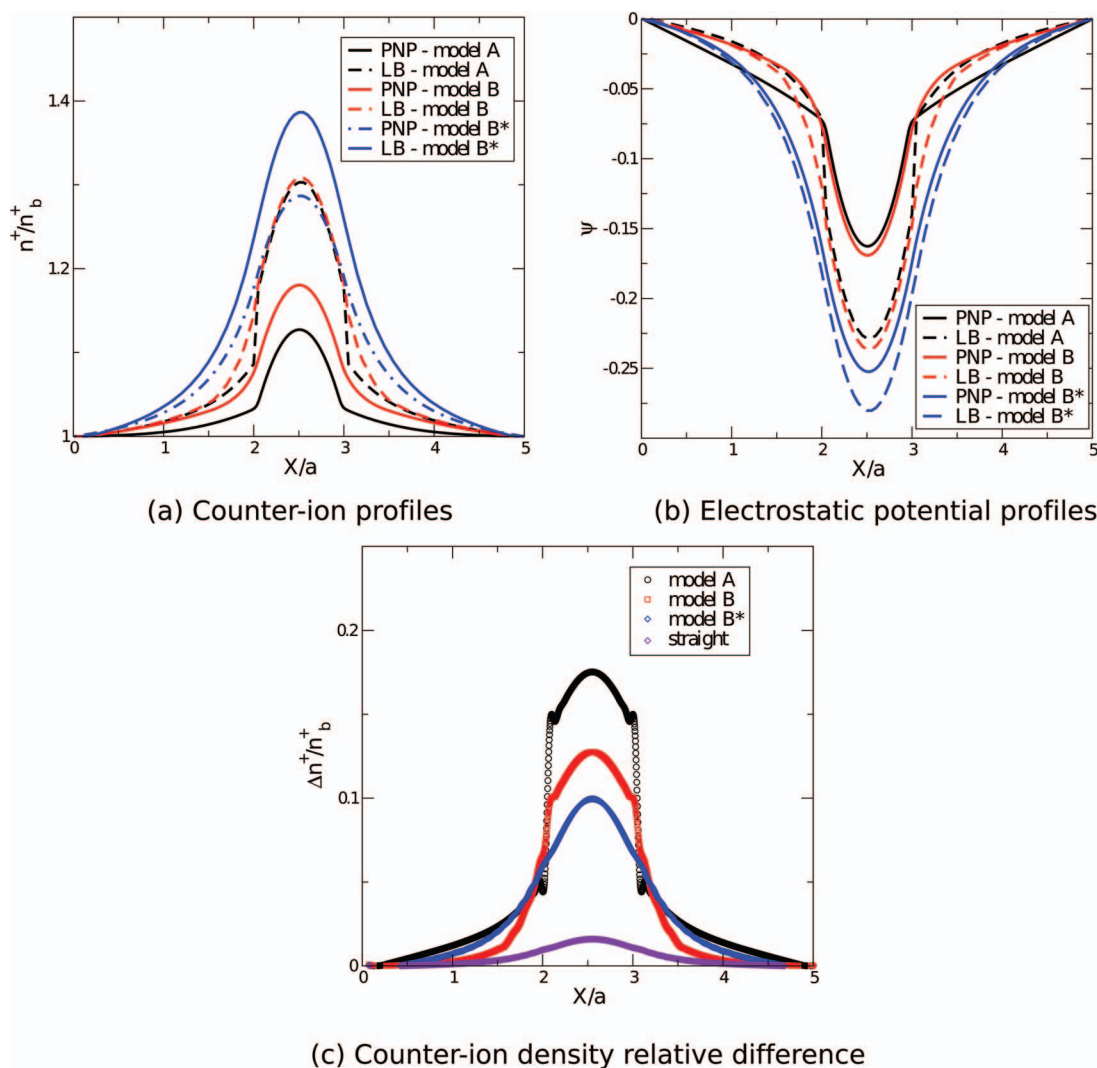


FIG. 6. Longitudinal profiles for system A ($d = 20$, $D = 60$, $a = 20$, and $A = 40$), system B with ($d = 20$, $D = 60$, $a = 20$, $r = 10$, and $A = 40$), and a smoother version labelled B* ($d = 20$, $D = 60$, $a = 20$, $r = 30$, and $A = 0$). Data refer to $\Delta V = 0$. Plot (a) reports the counter-ion density, plot (b) the electrostatic potential, and plot (c) the relative difference between the 3D-LB and 1D-PNP profiles. The latter plot includes the case of a channel with homogeneous radius ($d = 20$, $D = 20$, $a = 20$, and $A = 40$).

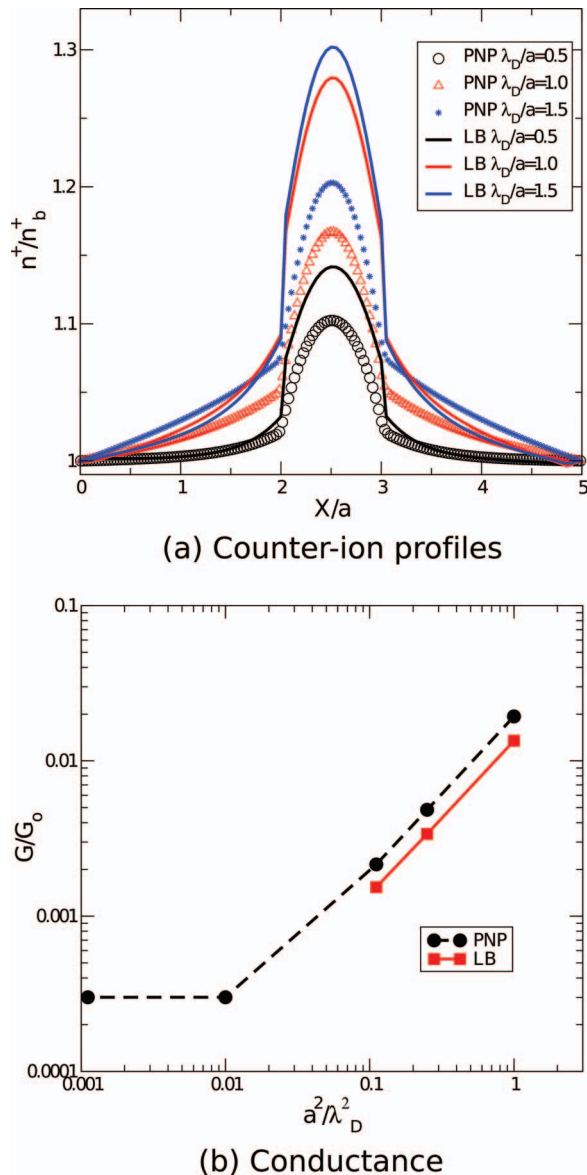


FIG. 7. Normalized profile of counter-ions and conductance at different Debye lengths as obtained with the 1D-PNP and 3D-LB methods for system A ($d = 20$, $D = 60$, $a = 20$, and $A = 40$) and $\Delta V = 10^{-2}$. The conductance is normalized by the value $G_0 = e^2 D / (a^2 k_B T)$.

The effectiveness of screening is a critical parameter in the channel region as it modulates the amount and spatial extension of the double layer induced by the surface charge. Due to the homogenization procedure, the radial charge polarization is neglected by the PNP equation, therefore any contribution stemming from electro-osmosis is absent at this level of the theory.

Fig. 7 reports the counter-ion density profiles for the different systems and various Debye lengths and associated conductances. As apparent, the quality of the PNP theory degrades with the increase of the Debye length, as expected. This degradation is visible both inside the channel region and in the reservoirs, where concentration polarization also depends on the screening attitude. At $\lambda_D = 10$, the maximum of counter-ions differs from the corresponding LB value by $\approx 5\%$, and at $\lambda_D = 30$ the relative difference is $\approx 10\%$.

In terms of conductance, the PNP solution provides fluxes larger by $\approx 30\%$ as compared to the LB data, and for $10 \leq \lambda_D \leq 30$, this relative difference does not depend on the Debye length. The mechanism for charge transport at PNP level can be ascribed to the Ohmic mechanism in this level of description, that is, in bulk conditions the conductance is linearly related to the number of (positive and negative) free charge carriers. On the other hand, in the full three-dimensional system the effect of the transverse charge polarization is to bind the charge carriers more strongly to the walls and modulated by the geometrical inhomogeneities in the longitudinal axis, thereby reducing effectively the passage of charges across the device as compared to a simple Ohmic mechanism. In principle, convection and the attendant electro-osmosis phenomenon could increase the level of ionic conduction, thereby having a lower conductivity in the PNP solution. Convection is taken into account in the LB description but is missing in the PNP theory. From the numerical data, it is apparent that at the chosen values of surface charge and Debye length, convection is a minor actor. Overall, our finding provides a simple scaling value of 30% to consider the PNP prediction on a semi-quantitative basis. More involved geometries, and different values of the surface charges and Debye length, however, may require a more accurate comparison between the 1D and the 3D solutions.

IV. CONCLUSIONS

The set of effective one-dimensional equations established in this paper represents a convenient route to the solution of full three-dimensional problems, which often require a demanding numerical effort. Entropic forces are not present in a simplistic one-dimensional version PNP equations, but they can be accounted for by a proper homogenization of the three-dimensional equations. The end result is a non-trivial dynamics where the modulation of surface charge and degree of confinement can be considered in effective terms. The 1D-PNP equation derived here is an extension of the Fick-Jacobs dynamics for diffusive processes to charged fluids.¹⁵

The method of homogenization finds applications in the analysis of charge transport in confined geometries and is a viable and efficient substitute of more detailed descriptions. It can be particularly useful in the study of transport of biological ion channels. In spite of the approximations involved, the method turns out to be useful because it offers a valid opportunity to deduce the main physical characteristics of ion transport in channels in a simple way.

The 1D-PNP description, however, can be used in a semi-quantitative way because as compared to the 3D solution it provides smaller counter-ion accumulations and co-ion depletion in the charged regions, by $\sim 10\%$. This mismatch increases with the degree of confinement and the Debye length. In terms of ionic conductance, the mismatch between 1D and 3D solutions can be as large as 30%, so that the PNP solution can be used for qualitative purposes only.

Regarding the approximation employed throughout the paper of neglecting electro-osmosis, as argued by Yossifon for overlapping double layers, as it occurs in narrow pores of nanometric size and not too concentrated solutions, the

contribution of electro-osmosis to the ion flux is subdominant with respect to the electrodiffusion contributions.³³

In conclusion, the homogenization procedure works well when the transversal density profile varies slowly, so that we can balance a boundary term with the average of the function over the section. The agreement between 3D-LB and 1D-PNP solutions improves for a channel entrance varying smoothly along the longitudinal direction. The reported phenomenology is particularly sensitive to the geometry of the pore mouth where the electric field generates an inhomogeneous charge distribution and polarization along the pore which can be relatively long ranged along the channel axis. Important consequences can arise in different contexts, such as in the study of supercapacitors as widely studied in recent years.³⁴ Although in super capacitors the porous electrodes operate at constant potential,³⁵ extending the proposed formalism to account for different boundary conditions does not constitute any fundamental limitation.

ACKNOWLEDGMENTS

U.M.B.M. acknowledges the support received from the European Science Foundation (ESF) for the activity entitled “Exploring the Physics of Small Devices (EPSD)” under the Grant No. 3720. Dr. Mauro Chinappi is kindly acknowledged for useful discussions. I.P. acknowledges financial support from MINECO (Spain) and DURSI under Project Nos. FIS2011-22603 and 2009SGR-634, respectively.

¹T. Squires and S. Quake, *Rev. Mod. Phys.* **77**, 977 (2005).

²I. Pagonabarraga, B. Rotenberg, and D. Frenkel, *Phys. Chem. Chem. Phys.* **12**, 9566 (2010).

³A. Malevich, V. Mityushev, and P. Adler, *J. Colloid Interface Sci.* **345**, 72 (2010).

⁴H. Daiguji, P. Yang, and A. Majumdar, *Nano Lett.* **4**, 137 (2004).

⁵I. Vlassioug, S. Smirnov, and Z. Siwy, *Nano Lett.* **8**, 1978 (2008).

⁶U. Marini Bettolo Marconi and S. Melchionna, *Langmuir* **28**, 13727 (2012).

⁷C. Moyne and M. A. Murad, *Int. J. Solids Struct.* **39**, 6159 (2002).

⁸M. Schmuck and M. Z. Bazant, preprint [arXiv:1202.1916](https://arxiv.org/abs/1202.1916) (2012).

⁹I. Kosińska, I. Goychuk, M. Kostur, G. Schmid, and P. Hänggi, *Phys. Rev. E* **77**, 031131 (2008).

¹⁰J. Cervera, B. Schiedt, R. Neumann, S. Mafé, and P. Ramírez, *J. Chem. Phys.* **124**, 104706 (2006).

¹¹J. Cervera, B. Schiedt, and P. Ramirez, *EPL* **71**, 35 (2005).

¹²W. E. Morf, *Anal. Chem.* **49**, 810 (1977).

¹³K. Kontturi, L. Murtoimäki, and J. A. Manzanares, *Ionic Transport Processes: In Electrochemistry and Membrane Science* (OUP, Oxford, 2008).

¹⁴M. Jacobs, *Diffusion Processes* (Springer-Verlag, New York, 1967).

¹⁵R. Zwanzig, *J. Phys. Chem.* **96**, 3926 (1992).

¹⁶P. Kalinay and J. Percus, *Phys. Rev. E* **74**, 041203 (2006).

¹⁷A. Berezhkovskii, M. Pustovoit, and S. Bezrukov, *J. Chem. Phys.* **126**, 134706 (2007).

¹⁸D. Reguera and J. Rubi, *Phys. Rev. E* **64**, 061106 (2001).

¹⁹U. Marini Bettolo Marconi and S. Melchionna, *J. Chem. Phys.* **126**, 184109 (2007).

²⁰A. Maggs, *EPL* **98**, 16012 (2012).

²¹C. L. Gardner, W. Nonner, and R. S. Eisenberg, *J. Comput. Electron.* **3**, 25 (2004).

²²D. Gillespie, W. Nonner, and R. S. Eisenberg, *J. Phys.: Condens. Matter* **14**, 12129 (2002).

²³S. Melchionna and U. Marini Bettolo Marconi, *EPL* **95**, 44002 (2011).

²⁴W. H. Press, B. P. Flannery, S. A. Teukolsky, and W. T. Vetterling, *Numerical Recipes in FORTRAN 77: The Art of Scientific Computing* (Cambridge University Press, 1992), Vol. 1.

²⁵S. Melchionna and U. Marini Bettolo Marconi, *EPL* **81**, 34001 (2008).

²⁶U. Marini Bettolo Marconi and S. Melchionna, *J. Chem. Phys.* **131**, 014105 (2009).

²⁷U. Marini Bettolo Marconi and S. Melchionna, *J. Chem. Phys.* **134**, 064118 (2011).

²⁸U. Marini Bettolo Marconi and S. Melchionna, *J. Chem. Phys.* **135**, 044104 (2011).

²⁹F. Capuani, I. Pagonabarraga, and D. Frenkel, *J. Chem. Phys.* **121**, 973 (2004).

³⁰B. Rotenberg, I. Pagonabarraga, and D. Frenkel, *Faraday Discuss.* **144**, 223 (2010).

³¹J. Sonnefeld, *Colloids Surf.* **108**, 27 (1996).

³²Q. Zou and X. He, *Phys. Fluids* **9**, 1591 (1997).

³³H.-C. Chang, G. Yossifon, and E. A. Demekhin, *Annu. Rev. Fluid Mech.* **44**, 401 (2012).

³⁴R. Kötz and M. Carlen, *Electrochim. Acta* **45**, 2483 (2000).

³⁵C. Merlet, B. Rotenberg, P. Madden, P. Taberna, P. Simon, Y. Gogotsi, and M. Salane, *Nature Mater.* **11**, 306 (2012).